2026 IEEE Transportation Electrification Conference & Expo (ITEC) & Electric Aircraft Technologies Symposium (EATS) (ITEC+EATS) | 979-8-3315-8773-4/26/$31.00 ©2026 IEEE | DOI: 10.1109/ITECEATS66641.2026.11593008

Gain-Scheduled Data-Enabled Predictive Control for EV Thermal Management

Wanqun Yang
ECE, Oakland University
Rochester, MI, USA
junchen@oakland.edu

Luke Nuculaj
ECE, Oakland University
Rochester, MI, USA
lukenuculaj@oakland.edu

Jun Chen*
ECE, Oakland University
Rochester, MI, USA
junchen@oakland.edu

***Abstract*—This paper presents a Gain-Scheduled Data-Enabled Predictive Control (DeePC) framework for a cell-level battery thermal management system. The system explicitly captures the electro-thermal coupling of individual cells and their heat exchange with the coolant, and divides the operation into multiple zones. To deal with the nonlinearity that is commonly present in battery systems, zone-specific Hankel matrices are constructed from simulation-generated data, allowing the DeePC controllers to adaptively schedule control gains according to the current thermal condition. Comprehensive simulation results demonstrate that the proposed approaches can effectively track target temperature and improves temperature uniformity across cells without an explicit system model.**

***Index Terms*—Electric vehicle, battery thermal management, data-enabled predictive control, gain scheduling.**

I. Introduction

As an effective solution to reduce carbon emissions, electric vehicles (EVs) are being increasingly adopted worldwide. However, in cold regions, their performance is limited due to the performance degradation of batteries under low-temperature conditions [1]–[3], which can cause long charging durations, limited driving range, and performance degradation [4]–[7]. At low temperatures, EV battery temperatures often drop well below the optimal operating range, which leads the reduced diffusion rate of lithium ions, the increased internal resistance, and the accelerated lithium plating that can significantly lower available capacity and efficiency [8]–[10].

To address these issues at low temperature, various battery thermal management systems (BTMS) have been developed. Conventional approaches generally rely on pack-level temperature regulation using PID control, while advanced methods have introduced model predictive control (MPC) to improve heating efficiency and energy balance [11]–[13]. However, most existing works treat the battery pack as a single thermal entity, neglecting the nonuniform temperature distribution that naturally arises along the coolant flow path. Such thermal gradients accelerate cell degradation and compromise both safety and performance. In addition, accurate electro-thermal modeling of battery packs remains challenging due to the strong nonlinear coupling between electrical behavior and heat generation. These dynamics vary significantly with operating conditions such as temperature, flow rate, and compressor speed. As a result, developing reliable model-based controllers often requires detailed system identification and parameter tuning, which can limit the applicability of conventional model predictive control approaches in practical battery thermal management systems.

Recently, data-driven control methods have attracted increasing attention as an alternative to model-based predictive control [14]. Among these methods, Data-Enabled Predictive Control (DeePC) directly constructs predictive models from measured input–output data using Hankel matrices, without requiring explicit system identification. Based on Willems' fundamental lemma from behavioral systems theory [15], DeePC enables trajectory prediction and control design purely from data, and has been successfully applied to several control problems in energy systems [16]–[18].

Gain scheduling is a commonly used strategy to address nonlinear system behavior by switching controllers designed for different operating conditions [19]–[21]. In DeePC framework, gain scheduling can be realized by constructing multiple predictive models from datasets collected in different operating regions. Each operating region is represented by a separate Hankel matrix that captures the local input–output behavior of the system. During operation, the controller selects the appropriate Hankel matrix according to the current system condition, allowing the DeePC controller to better capture nonlinear dynamics. This paper presents a Gain-Scheduled DeePC framework for a cell-level BTMS. The system explicitly captures the electro-thermal coupling of individual cells and their heat exchange with the coolant, and divides the operation into multiple temperature zones. Simulation results demonstrate that the proposed approach effectively reduces cell-to-cell temperature deviations and enhances overall thermal uniformity compared with conventional BTMS strategies.

The main contributions of this work are summarized as follows:

1) A Gain-Scheduled DeePC framework is developed for cell-level battery thermal management, where controllers are scheduled according to thermal conditions.
2) Four zone segmentation strategies are proposed based on the average battery pack temperature, enabling the construction of distinct Hankel matrices for different operating regions to capture local thermal dynamics.

This work is supported in part by National Science Foundation through Award #2237317. *Corresponding author: J. Chen.*

TABLE I
LIST OF STATES AND INPUTS FOR THE BTMS UNDER STUDY.

Notation	Physical meaning	unit
T_1, T_2	coolant temp. after or before HP	$^\circ C$
T_{1a}, T_{2a}	coolant temp. at the inlet or outlet of coolant Branch a	$^\circ C$
T_{1b}, T_{2b}	coolant temp. at the inlet or outlet of coolant Branch b	$^\circ C$
$T_{c1} - T_{c5}$	5 coolant temp. within the branch	$^\circ C$
$T_{b1} - T_{b7}$	7 battery cells temp.	$^\circ C$
$SOC_{(b_1\text{-}b_7)}$	7 battery cells SOC.	*N/A*
$\dot{m}_a$	battery Branch a coolant flow rate	kg/s
$\dot{m}_b$	battery Branch b coolant flow rate	kg/s
$\dot{m}$	total coolant flow rate	kg/s
n_{comp}	compressor speed	*rpm*

3) A comparative study between 1-zone and multi-zone DeePC configurations is conducted, demonstrating that the 1-zone controller yields inferior steady-state uniformity and tracking performance, which highlights the effectiveness of the proposed gain-scheduled structure.
4) By benchmarking with nonlinear model predictive control (NMPC) [22], simulation results verify that the proposed approaches successfully track the target temperature while reducing thermal gradient across cells.

The remainder of the paper is organized as follows. Section II introduces the thermal management system, the definition of operating zones based on temperature, and the DeePC formulation. Section III presents the four zone segmentation strategies and compares their performance through simulation results. Finally, Section IV concludes the paper.

II. SYSTEM AND ZONE BASED DEEPC

A. Battery Thermal Management System

Our BTMS is based on literature [22]. The plant is a nonlinear electro-thermal model of a seven cells battery pack with two coolant branches and a heat pump which is also presented in Fig. 1. The system states and control inputs are

$$x = [SOC_{(b_1\text{-}b_7)}, T_{(b_1\text{-}b_7)}, T_{(c_1\text{-}c_5)}, T_{1a}, T_{1b}, T_{2a}, T_{2b}]^\top,$$
$$u = [\dot{m}_a, \dot{m}_b, n_{comp}]^\top.$$

The states vector includes cell temperatures, coolant node temperatures and state of charge (SOC). Control inputs are the two branch flow rates and a compressor speed. They are summarized in Table I. This dynamic system is used to generate data used to construct Hankel matrices and validate the DeePC controllers, while DeePC itself uses purely data-driven prediction. More system dynamics information can be found in [22]. The dataset is generated through a single run simulation of a plant under persistently exciting inputs. Independent pseudorandom binary signals (PRBS) are applied to the two coolant branch flow rates, and a multi-sine signal with small random noise is used for the compressor speed. Control input and state data are then stored to build the Hankel matrices used in the DeePC framework. Furthermore, the dataset is divided into multiple operating zones, where each zone corresponds to a separate Hankel matrix. This excitation strategy provides sufficiently rich input variations for constructing DeePC Hankel matrices. The average battery pack temperature is then used as a measurable variable to identify the current zone in real time.

B. Data-Enabled Predictive Control

Recently, great strides have been made in the predictive control literature surrounding the use of Hankel matrices for real-time prediction in the absence of an explicit model [23], a paradigm extending from Willems' fundamental lemma in behavioral systems theory [15]. Specifically, a necessary and sufficient condition regarding the existence of a system trajectory as a linear combination of augmented Hankel matrix columns is provided. With this concept in mind, the predictive controller solves the following quadratic program at each time step:

$$\min_{\alpha} \; \|H_L\alpha - z_{\text{ref}}\|^2_{M_L} + \lambda_\alpha \|\alpha\|_2^2 \tag{1}$$

subject to

$$H_n\alpha = z_n \tag{2a}$$
$$A_z H_L \alpha \leq b_z, \tag{2b}$$

where $H_n := [U_n^\top \;\; Y_n^\top] \in \mathbb{R}^{n(n_u+n_y)}$ and $H_L := [U_L^\top \;\; Y_L^\top] \in \mathbb{R}^{L(n_u+n_y)}$ are the past and future Hankel matrices of the current zone, parameterized by the system order n and the prediction horizon L. α is the coefficient vector that reconstructs consistent trajectories. The reference vector ($z_{\text{ref}} = [u_{\text{ref}}, \, y_{\text{ref}}]^\top$) combines the desired future input and temperature trajectories over the prediction horizon. The weighting matrix M_L penalizes both the control effort and the temperature tracking error, and we include the regularization term $\lambda_\alpha\|\alpha\|_2^2$ in the objective function to penalize over-extrapolation of Hankel matrix trajectories. Moreover, we note that (1) is a dense formulation of standard DeePC quadratic programming (QP) problems, which inherently enforces the constraint $\bar{z}_{[0,p-1]} = H_L\alpha$. In effect, this isolates α as the sole optimization variable.

III. ZONE SEGMENTATION AND RESULTS

A. Numerical Analysis of Different Zone Settings

Four zone settings are defined to evaluate the effect of data partitioning on DeePC performance. All cases use the same dataset collected from a 7200-s simulation with a sampling time of $T_s = 5$ s, resulting in $N = 1440$ samples. The dataset is divided according to the average battery pack temperature, and each subset is used to construct the corresponding zone's Hankel matrices. To ensure continuity near the temperature boundaries, overlapping regions are introduced so that adjacent zones share several hundred samples. Four distinct controller setups are considered in this paper, summarized as follows.

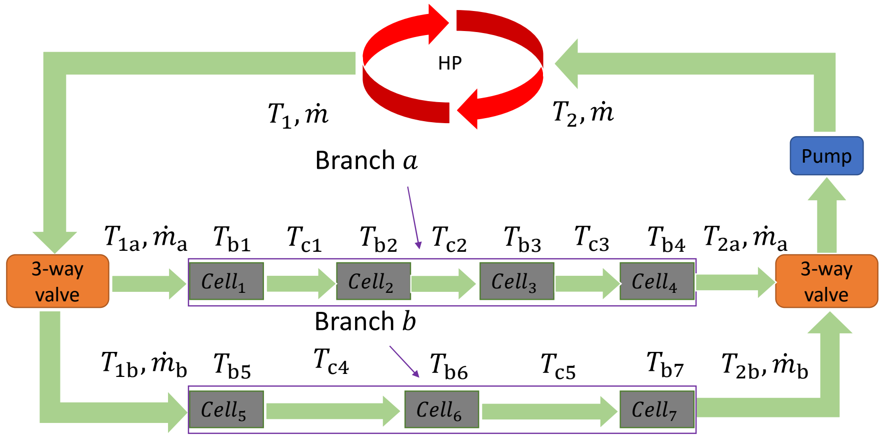

Fig. 1. Battery thermal management system under study.

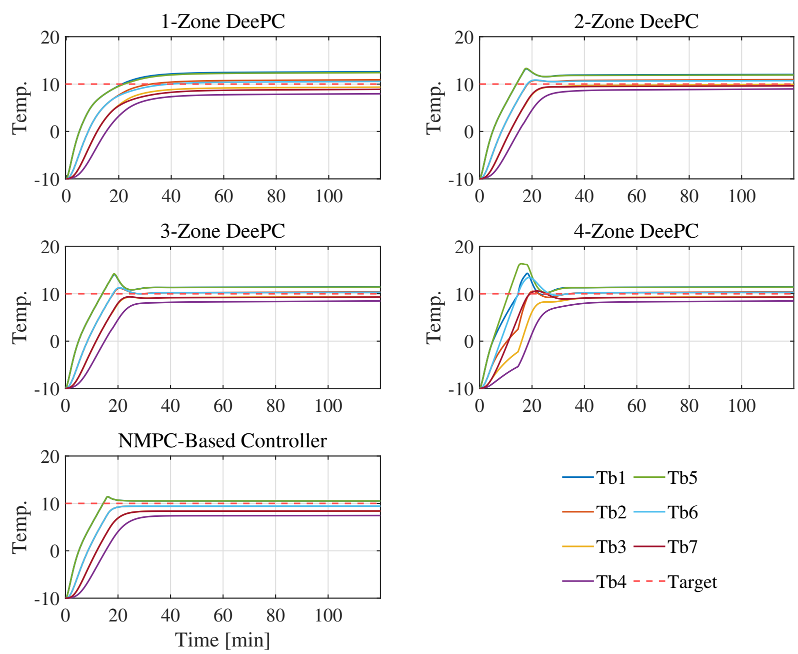

Fig. 2. Comparison of battery cell temperatures.

1-Zone DeePC: The dataset is used as a whole, and the Hankel matrices are constructed from all $N = 1440$ samples without segmentation.

2-Zone DeePC: The dataset is divided into a heating zone ($< 9°$C) and a stable zone ($> 9°$C). The average temperature reaches 9°C at sample 490. To avoid abrupt transitions between zones, 300 overlapping samples are included around the split point. As a result, the heating and stable zones contain approximately 790 and 1250 samples, respectively.

3-Zone DeePC: The dataset is divided into heating ($< 0°$C), transition (0°C–9°C), and stable ($> 9°$C) zones. The average temperature reaches 0°C and 9°C at samples 265 and 490. To maintain smooth boundaries, the heating zone extends 350 samples beyond the 0°C, while the transition zone overlaps 250 samples before and 200 samples after the two temperature thresholds. The stable zone begins 100 samples before the 9°C point and continues to the end of the dataset. Consequently, the heating, transition, and stable zones contain approximately 615, 675, and 1050 samples, respectively.

4-Zone DeePC: The dataset is divided into cold ($< -7°$C), heating ($-7°$C–5°C), transition (5°C–9°C), and stable ($> 9°$C) zones. The average temperature reaches $-7°$C, 5°C, and 9°C at sample indices 100, 356, and 490, respectively. The cold zone includes all samples up to index 100, with an additional 300-sample overlap to ensure data continuity, resulting in about 400 samples. The heating zone extends 50 samples

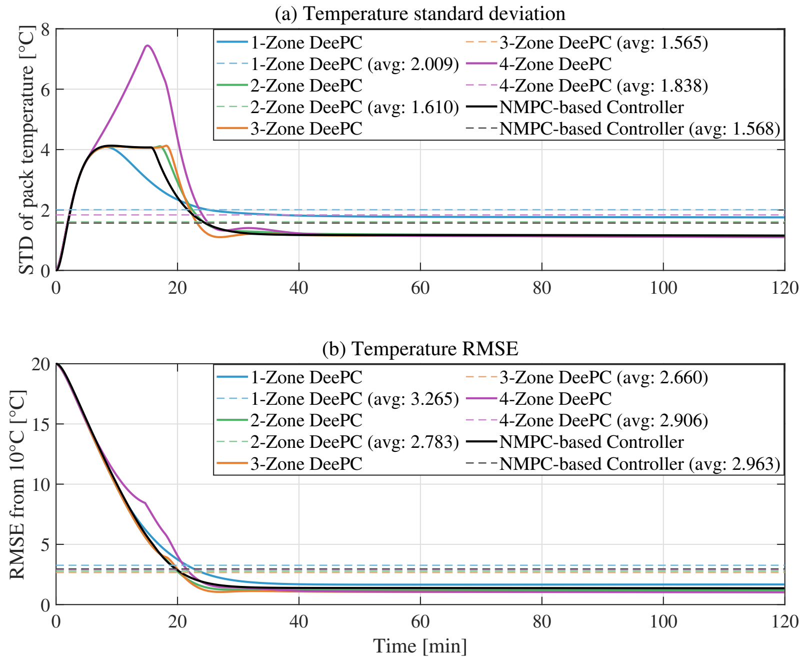

Fig. 3. Standard deviation and RMSE of cell temperatures.

before $-7°$C and 150 samples after $5°$C, giving approximately 556 samples in total. The transition zone includes 150-sample overlaps on both sides, yielding about 434 samples. The stable zone begins 100 samples before the $9°$C point and continues to the end of the dataset.

The reason for using a large overlap is to ensure that each zone contains sufficient data for constructing the corresponding Hankel matrices. In practice, if the overlap is too small or not included, the number of available samples near the zone boundaries can become insufficient, which may lead to poor prediction quality and degraded control performance. The zone boundaries are selected based on the average battery pack temperature so that different zones correspond to different thermal operating conditions during the heating process. The overlap size is therefore chosen to guarantee that each zone contains enough samples to construct the Hankel matrices with sufficient columns. In our simulations, overlaps of a few hundred samples provide stable control performance, whereas smaller overlaps often lead to insufficient data and may result in control failure.

After segmenting the dataset into temperature zones, we further verify that each zone contains a sufficiently large number of samples to construct the corresponding Hankel matrices. In particular, the number of available columns in each zone satisfies $N_c \gg (n_u+n_y)(n+L)$, ensuring adequate data coverage for trajectory reconstruction within the DeePC framework. In addition, numerical diagnostics show that the future Hankel matrix H_L is full row rank in all zones, indicating that the available data provide sufficient predictive capability for the DeePC controller.

B. Simulation Setting and Results

More details on the dataset generation are provided as follows. A training dataset is generated using the nonlinear 7-cell electro-thermal model. The sampling time of the simulation is 5 s, resulting 1440 samples. The dataset includes three control inputs, two coolant branch mass flow rates and the compressor speed, and seven output variables corresponding to the cell temperatures. The flow rates are excited by PRBS signals within 0-0.10 kg/s , while the compressor speed was varied within 100–4000 rpm using a multi-sine signal with small random perturbations. The nonlinear model is simulated at an initial temperature of $10°$C, and the resulting input–output trajectories are recorded for DeePC Hankel matrix construction.

In all simulations, the DeePC parameters are kept fixed across different cases. The sampling time is chosen as $T_s = 5$ s. The input vector has dimension $m = 3$, corresponding to the two branch flow rates and the compressor speed, and the output vector has dimension $p = 7$, corresponding to the seven cell temperatures. The past horizon and prediction horizon are set to $n = 20$ and $L = 10$, respectively. We benchmark the DeePC controllers with NMPC-based controller proposed in [22], which is implemented and solved using CasADi. It is worth noting that the NMPC settings, including the system model, actuator constraints, and cost function weights, are adopted as reported in [22].

The stage cost penalizes both input and temperature tracking. The reference temperature is fixed at $10°$C for all cells on the prediction horizon, and the input reference is set to $[0.08,\ 0.08,\ 1500]^\top$ for each step. The weighting matrix M_L

TABLE II
COMPARISON OF CONTROL PERFORMANCE OF DIFFERENT CONTROLLERS

Methods	T_{ss}**(min)**	σ_{tr}	σ_{ss}	σ_{all}	**RMSE**	t_{opt}**(sec)**
1-Zone DeePC	44.8	2.415	1.768	2.009	3.265	0.2359
2-Zone DeePC	**24.2**	3.238	1.199	1.609	2.783	0.1533
3-Zone DeePC	61.50	**1.984**	1.124	**1.565**	**2.660**	0.1158
4-Zone DeePC	62.83	2.488	**1.123**	1.838	2.906	0.1134
NMPC-based controller	∞	2.954	1.172	1.568	2.963	**0.0723**

is constructed as a block-diagonal matrix from the temperature and input weighting matrices over the prediction horizon. The temperature tracking weight is set to $q_y = 200$, and the input penalty uses a diagonal weighting matrix $Q_u = \mathrm{diag}(50, 50, 10^{-8})$ for the two branch flow rates and the compressor speed. A small regularization term $\lambda_\alpha = 10^{-1}$ on the DeePC coefficient vector is included. The control inputs are constrained by actuator bounds $0 \leq m_{b1}, m_{b2} \leq 0.10$ kg/s and $0 \leq n_{\mathrm{cmp}} \leq 4000$ rpm, with an additional constraint $m_{b1} + m_{b2} \leq 0.1$ kg/s enforced over the prediction horizon. No explicit input rate limits or thermal state constraints are imposed in this study. At each sampling time step, the past trajectory window is updated by appending the most recent input–output measurements to construct z_n. The QP is solved using MATLAB quadprog without warm-start.

Table II summarizes key metrics used for performance evaluation, where T_{ss} denotes the the first time step at which the average cell temperature reaches 10°C. The metric σ_{tr} represents the standard deviation of cell temperatures during the transient phase (i.e., before reaching 10°C), while σ_{ss} quantifies the spread after the average temperature stabilizes at the target. The overall temperature variation across the entire simulation is captured by σ_{all}. In all three cases, a lower σ value indicates more uniform thermal distribution among the seven battery cells. Notably, since the NMPC-based controller fails to reach the target temperature of 10°C, standard deviations are calculated with respect to the time point when the average battery pack temperature first reaches 9°C (rather than 10°C). RMSE is computed over the entire simulation horizon with respect to the reference value of 10°C, representing the average tracking error across all time steps. Compared to NMPC-based controller, it can be observed that the DeePC controllers with 2, 3, and 4 zones are able to heat the average battery pack temperature to the target value without significantly degrading pack uniformity and each of them shows some improvement in tracking error. t_{opt} refers to the average computation time per time step. Note that the computation time is measured on a standard desktop equipped with a 13th Gen Intel(R) Core(TM) i9-13900F processor and 32 GB of RAM. Although the NMPC with the CasADi solver achieves the lowest computation time of 0.0723 seconds, the absolute differences across the DeePC controllers remain small. Specifically, the deviations from the minimum are only 0.0810 seconds, 0.0435 seconds, and 0.0411 seconds for DeePC controllers with 2, 3, and 4 zones, respectively, which indicates that all controllers operate within a very low computational range. The 2-Zone DeePC controller reaches the target temperature the fastest but performs worse than 3-Zone DeePC in terms of pack uniformity, tracking error, and computation time. Compared to 3-Zone DeePC, 4-Zone DeePC does not provide further improvement. This is because a sufficient overlap between zones must be retained to ensure that each Hankel matrix contains enough information. As a result, increasing the number of zones does not necessarily lead to better performance.

Fig. 2 shows the temperature trajectories of all case studies in this work. Fig. 3(a) draws the standard deviation (STD) of cell temperatures during the simulation, performance of DeePC controllers with 2, 3, and 4 zones are close to NMPC-based controller, proves that they successfully improving temperature uniformity across cells without explicit system model. Fig. 3(b) presents the tracking RMSE across all controllers, showing that the DeePC controllers achieve performance comparable to or better than the NMPC-based controller. Considering both the STD and the tracking RMSE, the 1-zone DeePC exhibits a higher steady-state STD than the NMPC-based controller, and it is also the only DeePC configuration whose RMSE is slightly higher than that of the NMPC-based controller. This highlights the importance of the gain-scheduled Data-Enabled Predictive Control strategy in this study.

IV. CONCLUSIONS

A gain-scheduled DeePC framework for cell-level battery thermal management is proposed. By dividing the Hankel matrix into temperature dependent zones and constructing zone-specific Hankel matrices, the controllers adapt to varying dynamics from the simulation data. Results show that the 1-zone DeePC exhibits slightly inferior performance in terms of temperature uniformity and tracking accuracy compared with the multi-zone configurations, highlighting the importance of the gain-scheduled structure. Among the tested configurations, the 3-zone design achieves the best balance between tracking accuracy, thermal uniformity, and computational cost, proving that the proposed approach can successfully track the target temperature while reducing thermal gradient across cells.

REFERENCES

[1] M. Khaleel, Y. Nassar, H. J. El-Khozondar, M. Elmnifi, Z. Rajab, E. Yaghoubi, and E. Yaghoubi, "Electric vehicles in china, europe, and the united states: Current trend and market comparison," *International Journal of Electrical Engineering and Sustainability*, pp. 1–20, 2024.

[2] J. Chen, Z. Zhou, Z. Zhou, X. Wang, and B. Liaw, "Impact of battery cell imbalance on electric vehicle range," *Green Energy and Intelligent Transportation*, vol. 1, no. 3, p. 100025, 2022.

[3] L. Nuculaj and J. Chen, "Simultaneous cell state estimation via dense adaptive extended kalman filter," *IEEE Transactions on Control Systems Technology*, vol. 33, no. 6, pp. 2092–2107, November 2025.

[4] P. Xie, L. Jin, G. Qiao, C. Lin, C. Barreneche, and Y. Ding, "Thermal energy storage for electric vehicles at low temperatures: Concepts, systems, devices and materials," *Renewable and Sustainable Energy Reviews*, vol. 160, p. 112263, 2022.

[5] M. Senol, I. S. Bayram, Y. Naderi, and S. Galloway, "Electric vehicles under low temperatures: A review on battery performance, charging needs, and power grid impacts," *IEEE Access*, vol. 11, pp. 39 879–39 912, 2023.

[6] J. Chen, M. Liang, and X. Ma, "Probabilistic analysis of electric vehicle energy consumption using MPC speed control and nonlinear battery model," in *IEEE Green Technologies Conference*, Denver, CO, April 7–9, 2021.

[7] X. Zhang, Z. Li, L. Luo, Y. Fan, and Z. Du, "A review on thermal management of lithium-ion batteries for electric vehicles," *Energy*, vol. 238, p. 121652, 2022.

[8] N. Zhang, T. Deng, S. Zhang, C. Wang, L. Chen, C. Wang, and X. Fan, "Critical review on low-temperature Li-ion/metal batteries," *Advanced Materials*, vol. 34, no. 15, p. 2107899, 2022.

[9] N. Shidore and T. Bohn, "Evaluation of cold temperature performance of the JCS-VL41M PHEV battery using battery HIL," *Electric and Hybrid-Electric Vehicles–Batteries*, p. 133, 2008.

[10] G. Zhu, K. Wen, W. Lv, X. Zhou, Y. Liang, F. Yang, Z. Chen, M. Zou, J. Li, Y. Zhang *et al.*, "Materials insights into low-temperature performances of lithium-ion batteries," *Journal of Power Sources*, vol. 300, pp. 29–40, 2015.

[11] M. R. Hajidavalloo, J. Chen, Q. Hu, Z. Song, X. Yin, and Z. Li, "NMPC-based integrated thermal management of battery and cabin for electric vehicles in cold weather conditions," *IEEE Transactions on Intelligent Vehicles*, vol. 8, no. 9, pp. 4208–4222, 2023.

[12] R. Guo, L. Li, Z. Sun, and X. Xue, "An integrated thermal management strategy for cabin and battery heating in range-extended electric vehicles under low-temperature conditions," *Applied Thermal Engineering*, vol. 228, p. 120502, 2023.

[13] J. Chen, A. Behal, and C. Li, "Active battery cell balancing by real time model predictive control for extending electric vehicle driving range," *IEEE Transactions on Automation Science and Engineering*, vol. 21, no. 3, pp. 4003–4015, July 2024.

[14] W. Tang and P. Daoutidis, "Data-driven control: Overview and perspectives," in *2022 American Control Conference (ACC)*. IEEE, 2022, pp. 1048–1064.

[15] J. C. Willems, "The behavioral approach to open and interconnected systems," *IEEE Control Systems Magazine*, vol. 27, no. 6, pp. 46–99, 2007.

[16] L. Huang, J. Coulson, J. Lygeros, and F. Dörfler, "Decentralized data-enabled predictive control for power system oscillation damping," *IEEE Transactions on Control Systems Technology*, vol. 30, no. 3, pp. 1065–1077, 2021.

[17] W. Yu, Z. Tang, and W. Xiong, "Distributed robust data-enabled predictive control based voltage control for networked microgrid system," *Electric Power Systems Research*, vol. 231, p. 110360, 2024.

[18] L. Nuculaj, W. Yang, and J. Chen, "Robust data-enabled predictive control for EV charging under thermal constraints," in *IEEE Transportation Electrification Conference & Expo*, Novi, MI, June 10–12, 2026.

[19] J. Chen, "Extended kalman filter steady gain scheduling using k-means clustering," *International Journal of Modelling, Identification and Control*, vol. 34, no. 2, pp. 158–162, February 2020.

[20] J. S. Shamma and M. Athans, "Analysis of gain scheduled control for nonlinear plants," *IEEE Transactions on Automatic Control*, vol. 35, no. 8, pp. 898–907, 2002.

[21] Z. Xie, S. Li, P. K. Wong, W. Li, and J. Zhao, "An improved gain-scheduling robust MPC for path following of autonomous independent-drive electric vehicles with time-varying and uncertainties," *Vehicle System Dynamics*, vol. 63, no. 4, pp. 695–721, 2025.

[22] W. Yang, M. R. Hajidavalloo, Z. Li, and J. Chen, "NMPC-based cell-level thermal management of EV batteries in low temperature environment," *IFAC-PapersOnLine*, vol. 59, no. 30, pp. 1066–1071, 2025.

[23] J. Coulson, J. Lygeros, and F. Dörfler, "Data-enabled predictive control: In the shallows of the DeePC," in *2019 18th European Control Conference (ECC)*. IEEE, 2019, pp. 307–312.